Electron Scattering from the Deuteron and the Neutron-Proton Potential*

JOHN A. MCINTYRE AND SOBHANA DHAR†
High-Energy Physics Laboratory, Stanford University, Stanford, California
(Received February 28, 1957)

Electron scattering from the deuteron has been investigated experimentally at higher energies and larger scattering angles than before. Calculations have been made also for the scattering expected from deuterons with repulsive-core and with Yukawa-type neutron-proton potentials. As before, it is found necessary to introduce a proton size into the deuteron (or to modify the Coulomb interaction) in order to obtain agreement between the experimental results and the scattering calculations. Using the proton size determined by electron-proton scattering experiments, a comparison is made between the various calculated curves and the experimental data. It is found to be impossible to rule out either the repulsive-core or the Yukawa potentials.

I. INTRODUCTION

ELECTRON-SCATTERING experiments from the deuteron already have revealed a discrepancy between the deuteron size as measured by low-energy neutron-proton scattering and that measured by electron scattering.[1,2] Further experiments now have been performed at higher electron energies and at larger scattering angles. The results of these experiments would be expected to reveal more details of the deuteron structure. In order to analyze the data, several deuteron wave functions[3,4] which yield the correct deuteron binding energy, quadrupole moment, and triplet effective range have been used with the theoretical scattering formula of Jankus[5] to calculate the scattering from various possible deuteron structures. A comparison is made then between the experimental results and the various theoretical possibilities.

As was found before,[1] a large discrepancy appears between the experimental data and the scattering calculated from all possible theoretical deuterons. This discrepancy was removed before by assuming that the charge distribution of the proton in the deuteron had a root-mean-square radius of 0.8×10^{-13} cm. It was pointed out, however, that a modification of the Coulomb law of interaction between the deuteron and the scattered electrons at distances of 0.8×10^{-13} cm also could be used to remove the discrepancy. The same conclusions about the proton size were reached by Chambers and Hofstadter[6] in their analysis of experiments of electron scattering from the proton. The consistency of the deuteron- and proton-scattering results has been discussed by Yennie, Lévy, and Ravenhall.[2] Use will be made of this consistency in the following. The procedure adopted in this paper will therefore be the opposite of that adopted previously, i.e., the deuteron scattering experimental results plus the measured proton size as determined by electron-proton scattering will be used to determine the deuteron charge distribution, instead of using the deuteron-scattering experimental results plus the calculated deuteron charge distribution to determine the proton size. If this procedure is valid and the experimental data are sufficiently accurate, it should be possible to determine the deuteron charge distribution accurately enough to distinguish between various possible neutron-proton potentials in the deuteron.

For the sake of convenience, the procedure to be followed has been discussed in terms of a proton size. However, as mentioned above, a modification of quantum electrodynamics can just as well explain the electron scattering data. No preference between these two possibilities is implied in this paper although the point of view of a proton size will be used.

II. EXPERIMENTAL PROCEDURE

The experiments reported here were all performed with the electron-scattering apparatus at the end of the Stanford Mark III linear accelerator. This equipment has been described before.[1] All data were taken by using a high-pressure deuterium gas target (~2000 psi pressure). Experimental accuracy was limited to the same extent as before by the lack of reproducibility of the data ($\sim\pm10\%$).

Two new experimental difficulties appeared in extending the measurements to higher energies and larger angles than before. The first difficulty is caused by the saturation of the spectrometer magnet which is used for analyzing the energy of the electrons scattered from the target. It was found that the number of scattered electrons was not proportional to the area of the slit at the entrance of the magnet if this slit opening wsa too large. However, by decreasing the slit opening sufficiently, a constant ratio of counting rate to slit opening could be obtained. Because the deuteron recoil

* The research reported here was supported by the joint program of the Office of Naval Research and the U. S. Atomic Energy Commission, and by the U. S. Air Force through the Office of Scientific Research, Air Research and Development Command.
† Now at Lady Brabourne College, Calcutta, India.
[1] J. A. McIntyre, Phys. Rev. **103**, 1464 (1956).
[2] A theoretical analysis of this discrepancy is given by Yennie, Lévy, and Ravenhall, Revs. Modern Phys. **29**, 144 (1957).
[3] S. Gartenhaus, Phys. Rev. **100**, 900 (1955); wave functions kindly were supplied by S. Gartenhaus.
[4] H. Feshbach and J. Schwinger, Phys. Rev. **84**, 194 (1951); wave functions kindly were supplied by H. Feshbach.
[5] V. Z. Jankus, Phys. Rev. **102**, 1586 (1956).
[6] E. E. Chambers and R. Hofstadter, Phys. Rev. **103**, 1454 (1956).

increases with electron scattering angle, this saturation effect occurred only at the small electron-scattering angles where the scattered electrons have the highest energies. Therefore it was possible to use the large slit opening at the large scattering angles where the counting rate was low and a smaller opening at the small angles.

The second difficulty encountered in extending the measurements was the appearance of pulses in the counter not due to scattered electrons. These pulses presumably became apparent because of the lower counting rates obtained at the larger scattering angles. Some decrease in this background was obtained by changing from a Lucite Čerenkov counter (index of refraction 1.50) to a liquid $C_8F_{16}O$ Čerenkov counter (index of refraction 1.276).

The presence of this background is detected easily as shown in Fig. 1. The peak of elastically-scattered elec-

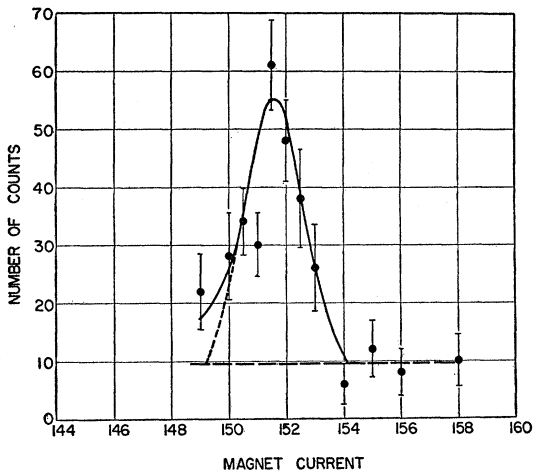

FIG. 1. Elastic electron-scattering data obtained at 80° and 400 Mev. The discriminator was set to count all electron pulses (low discriminator setting). Counts due to background appear on the high-energy side of the peak.

trons should drop to zero on the high-energy (high magnet current) side if no background is present. Counts at energies above the peak therefore indicate background. A subtraction can be made by extending the background region under the electron peak. However, this method may be rather inaccurate because of the low counting rates involved. Consequently, a second technique was used also to eliminate the background. A second pulse-height discriminator and scaler were driven in parallel with the usual discriminator and scaler. This second discriminator was set to accept only the largest pulses from the Čerenkov counter. When this was done, virtually no background pulses appeared. Figure 2 was taken simultaneously with Fig. 1 using the higher discriminator setting. Figure 3 shows the Čerenkov counter integral pulse-height distribution spectrum and indicates the discriminator settings for Fig. 1 and Fig. 2. This spectrum was taken at a small

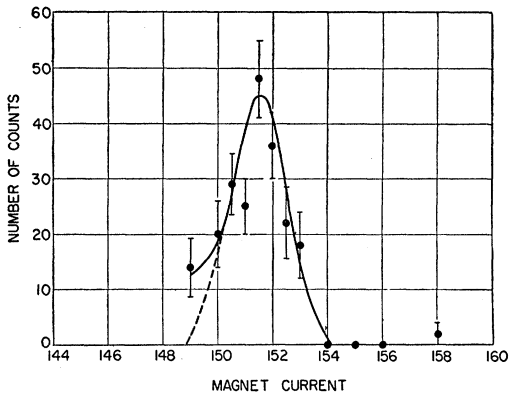

FIG. 2. Elastic electron-scattering data obtained at 80° and 400 Mev. The discriminator was set to count only the largest electron pulses (high discriminator setting). The background counts on the high-energy side of the peak have disappeared.

scattering angle where the counting rate was high enough to be convenient. There is virtually no background contribution at the small angles because of the high electron counting rates.

There are two disadvantages incurred in using the method of Fig. 2 instead of Fig. 1. First, the number of counts is smaller than in Fig. 1 (sometimes the high discriminator setting eliminated a large number of electrons along with the background). Second, the discriminator is set beyond the end of the "plateau" of the pulse-height distribution in Fig. 3; thus, any electronic drifts would be serious. In practice, it has been found that the data obtained for the two different discriminator settings are in good agreement and so an average of the results of Fig. 1 and Fig. 2 has been taken as the correct result. (The normalizing hydrogen point also was taken at both discriminator settings.)

The areas under the peaks shown in Figs. 1 and 2 were defined on the left by the dotted lines. These were drawn to be roughly symmetrical with the well-defined

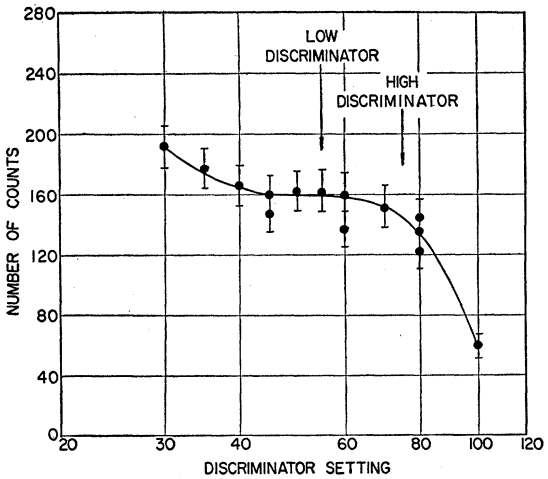

FIG. 3. The integral pulse height distribution obtained with the Čerenkov counter at small scattering angles.

curves determining the right side of the peaks. This procedure is valid here because the inelastic contribution to the scattering (points to the left of the dotted line) is approximately the same fraction of the elastic contribution at all scattering angles. Thus, the fraction of the inelastic scattering that extends under the elastic peak always is about the same and always small.

In converting the areas under the peaks in Figs. 1 and 2 to cross section values, it is necessary to convert the abscissa values which are in units of magnet current to units of beam displacement at the magnet exit slit.[7] This conversion is achieved by using the relationship between a current change in the spectrometer magnet and the resulting displacement of an electron trajectory at the exit slit of the magnet in front of the counter. This relationship was determined experimentally in two ways. (1) An essentially monoenergetic electron beam from the accelerator was introduced into the spectrometer. The spectrometer current was set so that the beam passed through the central trajectory of the spectrometer. A photograph of the beam spot at the exit of the magnet was then taken. Photographs were taken also with magnet currents set slightly higher and slightly lower than this value. The beam displacement then could be measured from the photographs and related to the known change in current. (2) From the kinematics of the electron-proton scattering process and the magnet currents found for the scattered electrons of various energies and angles, Chambers and Hofstadter[6] determined the relationship between magnet current and scattered electron energy. By then assuming a constant value for the magnet dispersion, $\Delta p/p$ (p=momentum), they obtained a relation between magnet current and beam displacement at the exit slit. Comparison of their results and those obtained by method (1) just described, showed agreement within $\pm 2\%$ except at the highest magnet currents. The largest discrepancy there was 7%. Later it will be shown by an internal consistency argument that the scattering data at the small angles do not contain any large systematic errors.

No corrections have been made for bremsstrahlung effects in the target. This correction is at most 2%.

The deuterium data were taken at 5° intervals between 30° and 90° at 400 Mev and between 30° and 80° at 500 Mev. Almost all measurements were repeated several times, some as many as five times. Cross sections were normalized by taking a hydrogen scattering run at 30° for the 400-Mev measurements, and at 45° for the 500-Mev measurements. The larger angle was chosen at 500 Mev so that the spectrometer magnet would not be saturated and therefore would give correct results for the largest entrance slit opening used. The hydrogen cross section was taken to be the product of (1) the cross section calculated by Rosenbluth[8] for electrons scattered by a point proton and (2) a (form factor)^2 term to account for the "finite size" of the proton. Using a proton charge density distribution of $\rho=\rho_0 re^{-r/a}$ with an rms radius of 0.78×10^{-13} cm,[6] the (form factor)^2 term is 0.819 for 30°, 400 Mev and 0.527 for 45°, 500 Mev. The normalizing cross sections are then (including radiative corrections)[9] $\sigma=440\times10^{-32}$ cm^2 sterad^{-1} for 30°, 400 Mev; and $\sigma=37.4\times10^{-32}$ cm^2 sterad^{-1} for 45°, 500 Mev.

The ratios F^2 of the experimental cross section to the point-charge cross sections [Mott scattering; see Eq. (1) in Sec. III] are plotted in Fig. 4 against q, the momentum transfer in the center-of-mass system. The 188-Mev and 400-Mev data presented before[1] are included also in the plots. Because of the validity of the Born approximation, the scattering is expected to be a function of q.[10]

A nice check on the accuracy of the experimental normalizations and the correctness of the analysis of the magnet spectrometer is the agreement between the 400-Mev and 500-Mev data when plotted against q as in Fig. 4. It is seen that within the accuracy of the measurements ($\sim\pm10\%$), the 400-Mev and 500-Mev data agree nicely. Since, for a given q, the magnet spectrometer is set for a different current for the 400-Mev scattering than for the 500-Mev scattering, the overlap of the 400-Mev and 500-Mev data indicates

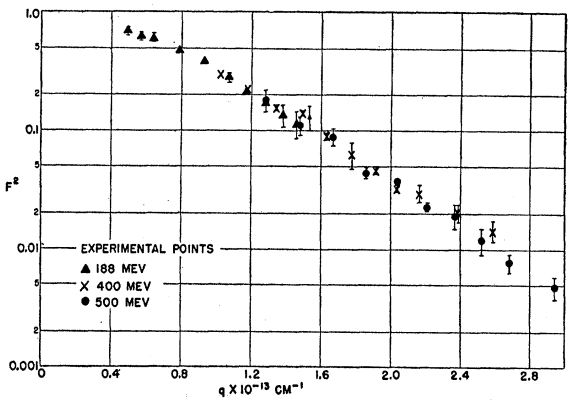

FIG. 4. Experimental data plotted against q, the momentum transfer in the center-of-mass system. The experimental cross sections have been divided by the Mott cross sections to make the plot. This ratio is designated F^2.

[7] The exit slit width of the spectrometer magnet determines the width of the bite taken of the scattered electron spectrum. The slit width is constant experimentally, but the relation between a change in magnet current and a displacement of a monoenergetic beam at the exit slit is not. Thus, the peaks of Figs. 1 and 2 should be plotted against "beam displacement at the exit slit" rather than against "magnet current" if the areas under the peaks are to represent the number of scattered electrons.

[8] M. N. Rosenbluth, Phys. Rev. **79**, 615 (1950).

[9] J. Schwinger, Phys. Rev. **76**, 790 (1949).

[10] Actually, the scattering from the magnetic moment of the deuteron is not a function of q. However, at the smaller scattering angles, the magnetic moment scattering is negligible and even for the largest angle measured at 188 Mev, the magnetic moment scattering would be expected to raise the data <10% above the 400-Mev data. At the largest 400-Mev angle measured, this effect is <5%.

that the magnet spectrometer is performing as predicted.

III. THEORETICAL CONSIDERATIONS

A. Deuteron Scattering Calculations

Jankus[5] has calculated the contributions to the electron scattering of the charge and magnetic moment for both the S and D states of the deuteron. His result is the following in the laboratory system:

$$d\sigma=\tfrac{1}{4}e^4\cos^2(\tfrac{1}{2}\theta)[p_0^2\sin^4(\tfrac{1}{2}\theta)]^{-1}\times[1+p_0\sin^2(\tfrac{1}{2}\theta)]^{-1}d\Omega\cdot F_d^2, \quad (1)$$

where

$$F_d^2=\left[\int(u^2+w^2)j_0(\tfrac{1}{2}qr)dr\right]^2+\left[\int 2w(u-8^{-\frac{1}{2}}w)j_2(\tfrac{1}{2}qr)dr\right]^2+\tfrac{2}{3}(\tfrac{1}{2}q)^2\{[2/\cos^2(\tfrac{1}{2}\theta)]-1\}\times\left[\int\{[(\mu_p+\mu_n)(u^2+w^2)-\tfrac{3}{2}(\mu_p+\mu_n-\tfrac{1}{2})w^2]j_0(\tfrac{1}{2}qr)+2^{-\frac{1}{2}}w[(\mu_p+\mu_n)(u+2^{-\frac{1}{2}}w)+3\times 8^{-\frac{1}{2}}w]j_2(\tfrac{1}{2}qr)\}dr\right]^2; \quad (2)$$

F_d is termed the form factor of the deuteron scattering. Here e is the charge of the electron; θ is the electron scattering angle; p_0 is the momentum of the incident electron; r is the coordinate of the charge in the deuteron; μ_p and μ_n are the magnetic moments of the proton and neutron in nuclear magnetons, respectively, and $\hbar$, c, and M, the nucleon mass, have been set equal to unity; u and w are defined by the ground state wave functions for the deuteron ψ_m:

$$\psi_m=(4\pi)^{-\frac{1}{2}}r^{-1}[u(r)+8^{-\frac{1}{2}}S_{np}w(r)]\chi_m, \quad m=0,\pm 1, \quad (3)$$

where $S_{np}=3r^{-2}(\boldsymbol{\sigma}_n\cdot\mathbf{r})(\boldsymbol{\sigma}_p\cdot\mathbf{r})-(\boldsymbol{\sigma}_n\cdot\boldsymbol{\sigma}_p)$ and χ_m is the triplet spin function. Pauli spin matrices for the neutron and proton are $\boldsymbol{\sigma}_n$ and $\boldsymbol{\sigma}_p$, respectively.

For convenience, Eq. (2) may be written in the abbreviated form

$$F_d^2=F_0^2+F_2^2+F_{\text{mag}}^2, \quad (4)$$

where F_0^2 is the spherically symmetric term, F_2^2 is the "quadrupole" term and F_{mag}^2 is the "magnetic" term resulting from scattering by the magnetic moment of the deuteron.

In order to use Jankus' formulas realistically, it is necessary to insert deuteron wave functions which give correctly the known properties of the deuteron, namely, the binding energy, the effective range of the neutron-proton potential, and the quadrupole moment. The percentage D state should also be fitted, but is quite uncertain (between 2 and 6%, or even more). Wave functions satisfying the above requirements have been obtained by a number of investigators. In the following, three of these functions have been used for making electron scattering calculations. The first wave function used was obtained by Gartenhaus[3] by applying the Chew-Low meson cutoff theory. Gartenhaus has found that the correct deuteron properties result by using the same parameters in the Chew-Low theory as those determined by the meson-nucleon scattering and the meson photoproduction experiments. An S-state repulsive-core potential with a core radius 0.65×10^{-13} cm and a core magnitude 1.4 Bev is derived using these parameters. Because this potential has been derived from a theory which yields correct results also for phenomena other than the properties of the deuteron, this potential has some theoretical significance. The other two wave functions used in the electron-scattering calculations are, in contrast, completely phenomenological. In each case Feshbach and Schwinger[4] used Yukawa potentials for both the S and D states to obtain the correct deuteron properties. The difference between these two cases results mainly in a difference in the percent D state in the deuteron.

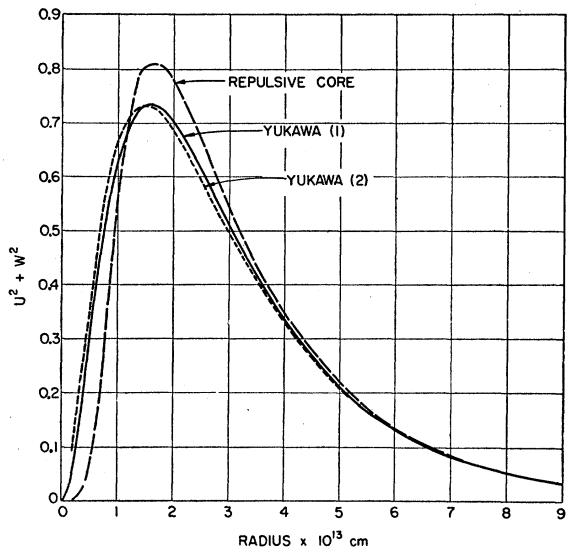

FIG. 5. Comparison of the "symmetric scattering" charge distributions of the three types of deuterons.

All three of the wave functions considered are plotted for comparison in Fig. 5, while Table I summarizes the deuteron properties obtained from the different wave functions. It is seen that the repulsive-core potential gives a rather large percent D state and a slightly high quadrupole moment in comparison to experiment. The two Yukawa potentials both yield deuteron properties fitting the experimental values closely. They differ only

TABLE I. Deuteron properties of the three wave functions used in the electron-scattering calculations.

Neutron-proton potential	Binding energy (Mev)	Triplet effective range (10^{-13} cm)	Quadrupole moment (10^{-27} cm^2)	Percent D state	Reference
Repulsive core	2.226	1.75	2.90	6.8	Gartenhaus[a]
Yukawa (1)	2.23	1.71	2.74	4.2	Feshbach and Schwinger[b]
Yukawa (2)	2.23	1.68	2.77	2.8	Feshbach and Schwinger[b]
Experimental	2.226±0.003	1.70±0.03	2.74±0.02	4±2	Blatt and Weisskopf[c]

[a] See reference 3.
[b] See reference 4.
[c] See reference 12.

in their "percent D state." The effect of the D state on the electron scattering thus can be isolated by comparing the Yukawa (1) and Yukawa (2) cases.

The wave functions for these three different potentials were inserted into Eq. (2) and numerically integrated to give the results shown in Figs. 6, 7, and 8. The curve notation is that given in Eq. (4) above. Thus, F_0^2 is the contribution of the spherically symmetric scattering; F_2^2, the "quadrupole" scattering, and F_{mag}^2, the magnetic moment scattering. Since F_{mag}^2 is not a function of q, it is necessary to plot F_{mag}^2 for each scattering energy of interest.

It is seen that the "symmetric" scattering from the repulsive-core deuteron drops off more rapidly than that from the two Yukawa deuterons. However, the larger D-state probability for the repulsive-core case contributes more to the "quadrupole" scattering than

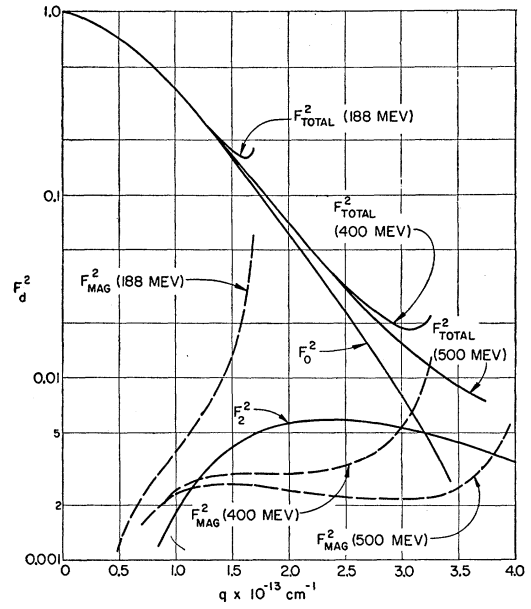

FIG. 6. Calculated F_d^2 values for scattering from the repulsive-core deuteron. Deuteron properties are shown in Table I; F_0^2 is the "symmetric" scattering, F_2^2, the "quadrupole" scattering, F_{mag}^2, the "magnetic moment" scattering, and F_{total}^2, the sum of the three scatterings.

the Yukawa D states do. Thus, the rather large difference between the repulsive core and the Yukawa "symmetric" scattering is somewhat compensated. Since the experimental data have been extended from[11] $q=2$ to $q=3$, the D-state scattering is seen to have become important.

Clearly, at large angles the scattering from the magnetic moment of the deuteron predominates. The increase in the magnetic-moment curves at large angles does not indicate an increase in magnetic-moment cross section, of course, but rather a decrease in the Mott-scattering cross section, which has been divided into all the cross sections to give the F_d^2 terms.

The total values for F_d^2 for all three cases are plotted in Fig. 9 for comparison. It is seen that there is as much as a factor of two difference between the scattering from

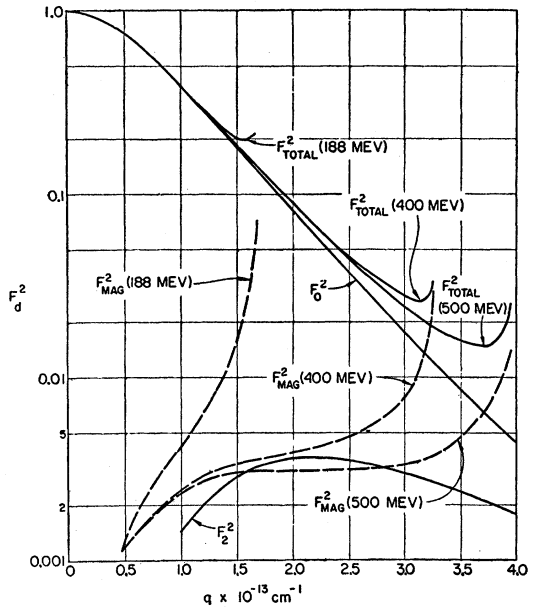

FIG. 7. Calculated F_d^2 values for scattering from the Yukawa (1) deuteron.

the repulsive-core and the Yukawa deuterons at $q=3$. The deviations introduced by the magnetic-moment scattering at large angles have not been included because they are small over the regions of experimental interest.[10]

B. Lower Limit on Deuteron Scattering

It is interesting, as will be seen later, to put a lower limit on the scattering curves of Fig. 9. This is done by the following argument due to Jankus. Figure 10 gives a plot of the square of $u=r\psi$ where ψ is a deuteron wave function; v^2 is the asymptotic value of u^2 extended back to the origin and normalized to unity there. Since the

[11] All distances are expressed in units of 10^{-13} cm.

effective range r_0 may be expressed[12]

$$r_0=2\int_0^\infty (v^2-u^2)dr,$$

the cross-hatched area in Fig. 10 is a measure of r_0.

In order to lower a deuteron scattering curve in Fig. 9, it is necessary to push the charge away from the origin while keeping the effective range r_0 fixed. This may be done in Fig. 10 by changing u^2 while keeping the cross-hatched area fixed; u_1^2 is a new possibility which pushes out the charge because the charge in area c has been transferred to area b which is at a greater radius. If the areas c and b are equal, r_0, of course, will remain unchanged. Clearly, the limit to this procedure is when u^2 becomes a vertical line at some radius a ($a=1.08$, for $r_0=1.70$),[12] and then follows v^2 to $r=\infty$. The scattering from such a charge distribution has been plotted in Fig. 9 over the range of q-values where the deuteron S-state scattering is dominant. This is the lowest scattering curve possible for a deuteron with an effective range of 1.70.[13]

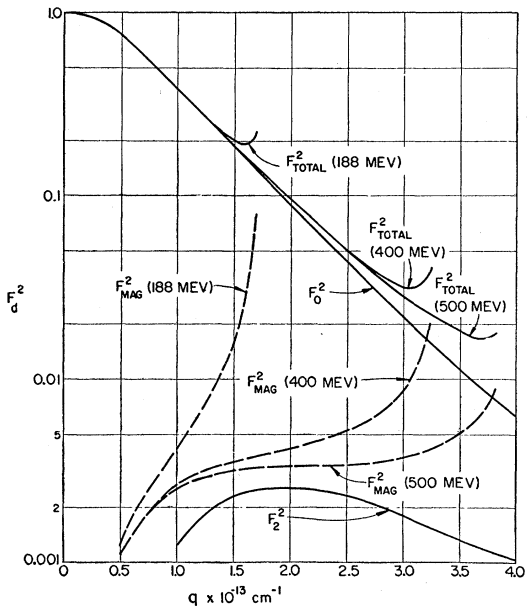

FIG. 8. Calculated F_d^2 values for scattering from the Yukawa (2) deuteron.

C. Effects of Nucleon Sizes

It is necessary now to determine the effect of the nucleon sizes on the electron scattering from the deuteron. The effect of the nucleon sizes will be to modify

[12] J. M. Blatt and V. F. Weisskopf, *Theoretical Nuclear Physics* (John Wiley and Sons, Inc., New York, 1952), Chap. II.

[13] R. G. Newton, Phys. Rev. **105**, 763 (1957), has shown that for longtailed potentials (potentials extending a distance larger than the neutron-proton triplet scattering length), a lower scattering curve can be obtained.

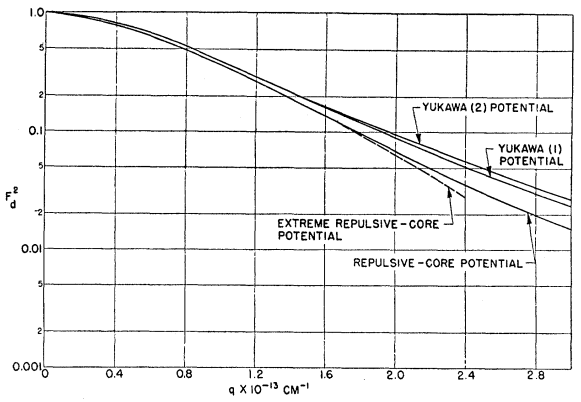

FIG. 9. Combined plot of the calculated total scattering F_d^2 from the three types of deuterons. The dotted curve represents the lower limit for the scattering from a deuteron with the correct effective range.

Eq. (2) which has been derived for point nucleons. There are three ways in which the neutron and proton in the deuteron may be extended: by the proton charge, the proton magnetic moment, or the neutron magnetic moment. The neutron charge does not appear in Eq. (2) since the charge of a point neutron is zero, and so the neutron charge extension need not be considered here. For the special but experimentally important case of the proton charge and magnetic moment and the neutron magnetic moment having the same extension, the form factor F for a deuteron containing extended nucleons may be expressed as

$$F=F_n\times F_d, \tag{5}$$

where F_n is the form factor for the extended proton or neutron, while F_d is the deuteron form factor as given in Eq. (2). This simple relationship results from folding the extended nucleon charge (or moment) distribution into the deuteron charge (or moment) distribution. Since the form factors, the F's, are Fourier transforms of the charge distributions, the folding of the charge distributions results in a multiplication of their Fourier transforms, the F's. The value $F_n(q)$ is calculated easily from the known nucleon density distribution since it is the Fourier transform of that distribution. In the following analysis of the experimental data, Eq. (5) will be used for introducing the effect of nucleon sizes.

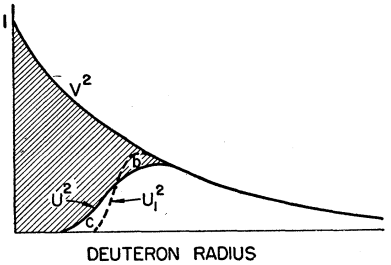

FIG. 10. Deuteron charge distributions for a given effective range value.

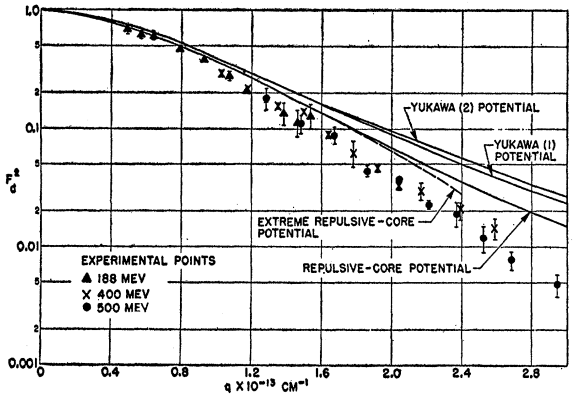

FIG. 11. Comparison of the experimental data with the calculated scattering. The dotted curve is the lower limit for the calculated scattering.

IV. DISCUSSION OF RESULTS

A. Comparison between Calculations and Experimental Results

The experimental results of Fig. 4 are plotted in Fig. 11 along with the theoretical curves of Fig. 9. The extreme repulsive-core curve represents the lower limit for scattering from the deuteron (see discussion in Sec. III). The large discrepancy that was noted before[1] for q values[12] less than 2 is seen to persist for q values up to 3.

Methods of removing this discrepancy have already been discussed.[1] It was shown that only a large change in the deuteron effective range (16 ± 5 times the standard deviation in the experimental effective range value) would yield agreement between a deuteron curve and the experimental data; however, agreement could be obtained by postulating a proton charge extension and a point neutron in the deuteron. The charge extension required was found to agree with the proton charge radius as measured by Chambers and Hofstadter,[6] while the point neutron assumption agrees with the various neutron-electron scattering measurements.[14]

In the following discussion, nucleon sizes will be introduced into the deuteron using values from these other experiments. A comparison will be made then to determine which of the modified deuteron curves best fits the experimental data.

B. Introduction of Nucleon Sizes

The effect on the electron-deuteron scattering of having extended nucleons in the deuteron has been discussed in Sec. III, C, and is given by Eq. (5). To determine $F_n(q)$, the nucleon form factor in Eq. (5), the results of other electron scattering experiments were used. From their electron-proton experiments, Chambers and Hofstadter[6] found that several proton radial charge distributions fit their data. Their best fit was obtained with a "hollow exponential" proton with a radial dependence of $\rho=\rho_0 re^{-r/a}$ and an rms radius value of 0.78 ± 0.05. Chambers and Hofstadter[6] have also measured the magnetic moment distribution of the proton and find that the distribution is virtually the same as that for the charge distribution. In addition, Blankenbecler, Hofstadter, and Yearian[15] have made a preliminary measurement on the magnetic moment distribution of the neutron. Their preliminary result is that the rms radius of the neutron magnetic moment has a value of 0.6 ± 0.2.

It is seen that within the experimental errors, the extension of the proton charge and magnetic moment and the extension of the neutron magnetic moment are equivalent. In the following, therefore, all will be assumed to have the same radial dependence and rms radius as the proton charge distribution, i.e., a "hollow exponential" radial dependence and an rms radius value of 0.78 ± 0.05. The Fourier transform of this distribution gives then, $F_n(q)$, the nucleon form factor.

The F_d^2 for various deuterons are the curves already plotted in Fig. 11. Multiplying these curves by F_n^2 as indicated by Eq. (5) gives the F^2 values plotted in Fig. 12. It is apparent immediately that the introduction of nucleon sizes has brought the calculated curves and the experimental points into virtual agreement. The various energy curves due to the effect of the non q-dependent magnetic-moment scattering (see Figs. 6, 7, and 8) have not been plotted in Fig. 12 because there is very little difference between the curves where there are experimental data.[10]

Finally, the overwhelming effect of the proton charge extension should be noted. Inspection of Figs. 6, 7, and 8 shows that only at the largest scattering angles is the

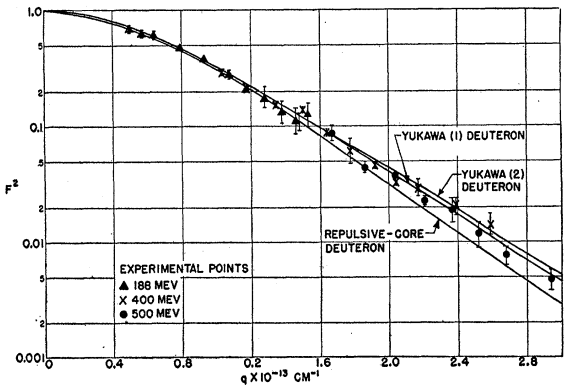

FIG. 12. Comparison of the experimental data with the calculated scattering modified for the effect of the finite size of the nucleons in the deuteron. The charge and magnetic moment of the proton and the magnetic moment of the neutron have been given rms radii of 0.78 and a "hollow exponential" radial dependence of $re^{-r/a}$. The neutron charge distribution is considered as a point.

[14] Melkonian, Rustad, and Havens, Bull. Am. Phys. Soc. Ser. II, 1, 62 (1956); Hughes, Harvey, Goldberg, and Stafne, Phys. Rev. 90, 407 (1953).

[15] R. Hofstadter, Revs. Modern Phys. 28, 247 (1956), and private communication.

scattering of the deuteron magnetic moment important. In fact, at the largest 188-Mev angle measured, the magnetic contribution is less than 10%; at the largest 400-Mev angle, less than 12%; at the largest 500-Mev angle, less than 12%. These percentages drop rapidly at the small scattering angles. Thus, the parameters used to extend the magnetic moments of the nucleons are not very critical. In other words, it is the charge extension of the proton that introduces virtually all of the modification to the point-nucleon deuteron scattering. In the following discussion, therefore, the term "proton charge extension" will be used although the proton and neutron magnetic moments are assumed to have the same extension also.

C. Determination of the Neutron-Proton Potential

By weighing the various experimental points according to the uncertainties shown in Fig. 12, a statement

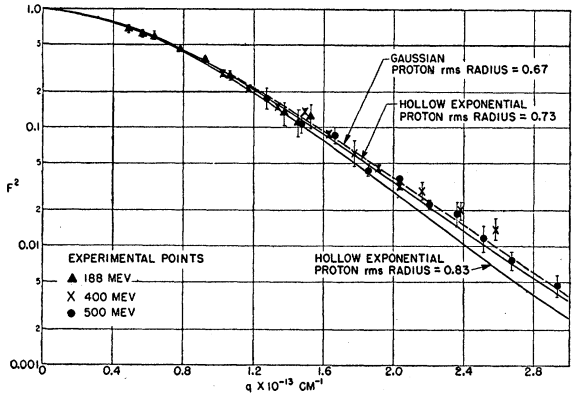

FIG. 13. Comparison of the experimental data with the calculated scattering from the repulsive-core deuteron. Solid curves are for "hollow exponential" protons with rms radii of 0.73 and 0.83; the dotted curve is for a Gaussian proton with rms radius of 0.67.

can be made concerning the fit between the points and the different curves. These fits are as follows: The repulsive-core curve is 8.2 standard deviations away from the average of the combined experimental data, the Yukawa (1) curve is 1.2 standard deviations, the Yukawa (2) curve is 5.6 standard deviations. Thus, the Yukawa (1) curve is by far the best fit.

However, this conclusion has to be relaxed because of the uncertainty in the radius of the proton charge distribution. Figure 13 shows the effects of using with the repulsive-core potential, a proton charge having the extreme radii allowed by the electron-proton scattering experiments. The 0.73-radius proton case clearly fits better than the 0.83-radius case, but is still too low by 4.7 standard deviations. However, if the uncertainty in the proton charge shape is introduced also, a still better fit can be obtained. If the radial distribution of the proton charge is assumed to be Gaussian, for example, instead of "hollow exponential,"

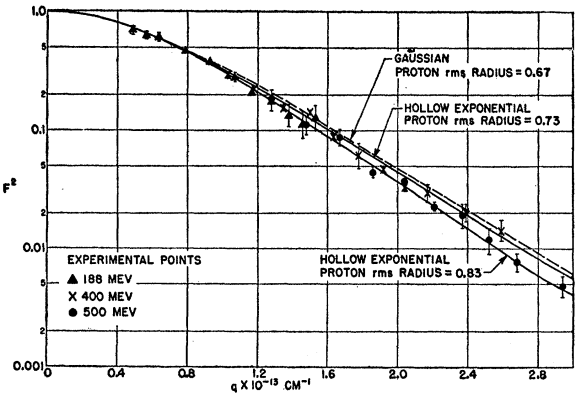

FIG. 14. Comparison of the experimental data with the calculated scattering from the Yukawa (1) deuteron.

then the rms radius is 0.72 ± 0.05.[6] Taking the smallest allowed value of the radius, 0.67, and a Gaussian form factor, the dotted curve in Fig. 13 is obtained. This curve is only 1.1 standard deviations low, and so may be said to fit.

A similar analysis may be carried out for the Yukawa (1) and the Yukawa (2) cases. The curves obtained are plotted in Figs. 14 and 15. The Yukawa (1) case already has been seen to fit the 0.78 radius "hollow exponential" proton, while the Yukawa (2) case fits with a 0.83 radius "hollow exponential" proton.

It may be concluded, therefore, that while the Yukawa (1) case is the only fit possible using the expected value for the proton charge size in the deuteron, there is enough uncertainty in the shape and size of the proton charge to allow a fit to be made to the repulsive-core deuteron and the Yukawa (2) deuteron. To make this statement more precise, the values in Table II were computed. These values show how the uncertainty in the experimental determination of the proton charge radius encompasses the range of proton radii deduced from the electron-deuteron scattering experiments.

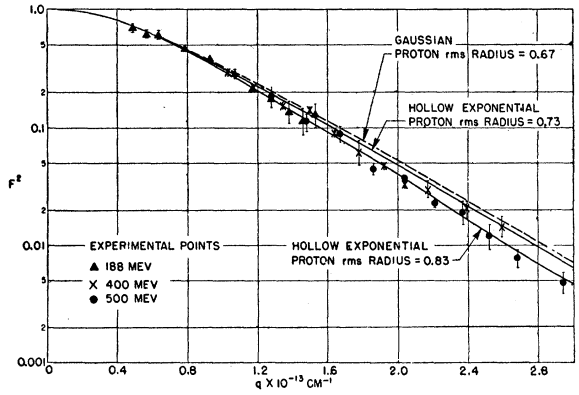

FIG. 15. Comparison of the experimental data with the calculated scattering from the Yukawa (2) deuteron.

TABLE II. Comparison of the proton charge radius deduced from various neutron-proton potentials and the electron-deuteron scattering experiments with the proton charge radius measured by electron-proton scattering experiments.

Kind of deuteron assumed	Radius and type of proton required to fit the data	
	Hollow exponential	Gaussian
Repulsive core	0.68±0.02[a]	0.66±0.02
Yukawa (1)	0.80±0.02	0.77±0.02
Yukawa (2)	0.84±0.02	0.80±0.02
Electron-proton scattering experiments[b]		
	0.78±0.05[c]	0.72±0.05

[a] Uncertainties in the radius are plus or minus one standard deviation.
[b] See reference 6.
[c] Uncertainties in the radius are not determined in terms of standard deviation.

D. Possibility of Other Neutron-Proton Potentials

It should be emphasized at this point that no evidence has been presented yet to show that an electron-scattering experiment can ever distinguish between a repulsive-core and a Yukawa-type deuteron. To show that such a distinction is possible, a number of repulsive-core and Yukawa deuteron wave functions should be calculated and the electron-scattering form factors computed. If, when this has been done, all of the repulsive-core form factor curves lie below any of the Yukawa curves, then a sufficiently accurate electron-scattering experiment should be able to distinguish between the two types of potentials.

Progress has been made already in this direction. Calculations of 81 different deuteron wave functions have recently been made by Blatt.[16] When the electron-scattering form factors from these deuterons have been computed, a good indication of the fruitfulness of electron-scattering experiments should be available. If it then proves possible in principle to distinguish between potential shapes, sufficiently accurate experiments may yield, in addition, information about the "percent D state" in the deuteron (see Figs. 6, 7, and 8).

E. Other Effects

From a meson-theoretical viewpoint, the deuteron is a complicated structure. There is the question, therefore, whether a simple potential analysis of the deuteron is sufficient or whether there will be scattering effects due to mesons being emitted, absorbed, or exchanged. Bernstein[17] has considered exchange effects and finds that for the larger q values, there should be the order of 10% addition to the scattering due to meson exchange. This would be in the direction to produce better agreement with the repulsive-core curve and the data in Fig. 12.

Another possible theoretical contribution to the scattering would be the dispersion scattering. This possibility has been considered by Schiff[18] and by Valk and Malenka[19] and has been shown to be of the order of only one percent.

V. CONCLUSIONS

Further data extending the scattering region from $q=2$ to $q=3\times10^{13}$ cm^{-1} verify the earlier conclusions that the finite size of the proton charge distribution must be introduced in calculating the electron scattering from the deuteron. This proton size effect (or equivalently, the effect of a modification of the Coulomb law at small distances) reduces the scattering cross section a factor of five at $q=3$. A discussion of the implications of the effect already has been given.[1,2]

Using the proton charge radius determined by electron-proton scattering experiments,[6] the experimental data are found to fit well a deuteron with a Yukawa-type potential. However, introduction of the allowed uncertainty into the proton charge radial distribution permits a repulsive-core deuteron to fit the data also. The experiments therefore do not distinguish between the Yukawa and the repulsive-core potential.

ACKNOWLEDGMENTS

The authors wish to thank Professor Robert Hofstadter for his many contributions to this work and for a number of helpful discussions. Dr. D. G. Ravenhall has contributed greatly in setting up the scattering calculations and in clarifying many theoretical points. We also would like to thank Dr. Franz Bumiller for help in calibrating the magnet, Mrs. Paul Byrd for making some of the calculations, and the accelerator crew under Professor R. F. Mozley for the reliable performance of the accelerator.

[16] J. M. Blatt (private communication).

[17] J. Bernstein, Phys. Rev. **104**, 249 (1956).
[18] L. I. Schiff, Phys. Rev. **98**, 756 (1955).
[19] H. S. Valk and B. J. Malenka, Phys. Rev. **104**, 800 (1956).